Master's Thesis

Synthesis of highly transparent photoresist for ultrathick patterns

Sun-Young Yu

Department of Energy Engineering

(Energy Engineering)

Graduate School of UNIST

2018

Synthesis of highly transparent photoresist for ultrathick patterns

Sun-Young Yu

Department of Energy Engineering

(Energy Engineering)

Graduate School of UNIST

Synthesis of highly transparent photoresist
for ultrathick patterns

A thesis/dissertation

submitted to the Graduate School of UNIST

in partial fulfillment of the

requirements for the degree of

Master of Science

Sun-Young Yu

06. 15. 2018

Approved by

_____

Advisor

Ji-Hyun Jang

Synthesis of highly transparent photoresist
for ultrathick patterns

Sun-Young Yu

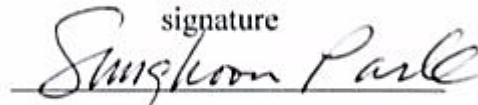This certifies that the thesis/dissertation of Sun-Young Yu is approved.

06. 15. 2018

signature

_____
Advisor: Ji-Hyun Jang

signature

_____
Sunghoon Park

signature

_____
Ji-Wook Jang

Abstract

Interference lithography allows to fabricate large-area, defect-free multidimensional submicron structures. Multidimensional periodic structures made by interference lithography are used in a variety of applications such as photonic crystal, data storage and energy device. Recently, ultrathick structure with a high aspect ratio has received a lot of attention for a board range of applications including opto-electronics, biomechanics, and nanointerfaces tuning for surface wetting/dewetting. Interference lithography uses novel photoresists with high mechanical stability and transparency. SU-8 is representative negative photoresist and it has been broadly used. However, SU-8 is difficult to fabricate thick patterns with good resolution. The intensity of UV light at the bottom of the thick SU-8 photoresist film is reduced due to high absorbance of SU-8 in the UV region. Polyhedral oligomeric silsesquioxane (POSS) is one of the interesting materials with ultrahigh transparency, good thermal and mechanical stability. However, POSS-based photoresist has a lower glass transition temperature (T_g) than room temperature. POSS-based photoresist has difficulty in the lithography process since resin remains in a liquid phase. This report introduces a solid state POSS-based photoresist for fabricating ultrathick submicron structure. Poly (glycidyl methacrylate-co-acryloisobutyl POSS) (PGP) is synthesized through polymerization of acrylate polymer containing epoxy group and POSS functionalized with an acrylate group. PGP has an ultrahigh transmittance of light in UV-vis region (96.6 % at 355 nm of the films with the thickness of 100 μm), a high T_g (~72.2 °C), and enhanced mechanical properties (Hardness of 0.16 GPa and Young's modulus of 6.09 GPa). Due to these properties, PGP is superior to SU-8, conventional photoresist, for fabricating ultrathick patterned structures via interference lithography. An ultrathick PGP patterned structure provides potential in a variety of applications. Solar desalination, one of the applications, is a technique to desalinate water using solar energy. In this technique, the active material absorbs sunlight and convert it thermal energy. One of factors to enhance solar desalination efficiency is broadband absorption of sunlight. An ultrathick PGP patterned structure helps the light trapped by increasing the light traveling through the active material. As a result, an active material including ultrathick PGP patterned structure greatly enhances solar desalination efficiency.

Contents

List of figures

8

List of Tables

I.   Introduction

1.1 Fabrication of patterned structure

1.1.1   Interference lithography

Two- or three-dimensional structures with submicron-scale periodic patterns have received a lot of attention in a wide range of applications such as data storage, energy devices, photonic crystals and sensors.[1-5] Nanopatterned structures fabricated through a variety of fabrication methods including nanoimprint lithography, photolithography, and self-assembly have been extensively studied for the applications I mentioned.[6,7] Interference lithography is one of the most dominant yet relatively inexpensive methods for fabricating large-area structures with the periodic pattern. This technique utilizes the principle of interference of several times of coherent laser beams. **Fig 1a** shows experimental arrangement which is one of the two widely used methods of two-beam interference lithography. It is a Lloyd's mirror configuration which utilizes mirror interferometer. A SEM image in **Fig 1b** shows 1D structure is created by interfering two coherent beams, one is the incident beam and second is the reflected beam by the mirror. 2D structures with a square array of posts can be fabricated by double exposure with along the x-direction and y-direction, respectively, as shown in **Fig 1c**. More complex periodic structures can fabricate by multi-beam interference lithography.[8]

1.1.2   Photoresist

Interference lithography utilizes novel photoresist with high transparency and mechanical properties. The typical conventional negative-tone photoresist is SU-8. It has excellent thermal stability, high mechanical property, and good chemical and electrical resistance. So, SU-8 is commercially available and has been extensively utilized to produce thick submicron structures with excellent contrast.[9] However, It has problems including large volume shrinkage, difficulty in the elimination either by a solvent- or heat treatment due to high absorption in the UV region. This makes it difficult to produce submicron patterns over 100 um with good contrast. Among the problems, the absorption of SU-8 is a critical obstacle to manufacturing ultra-thick submicron patterns with good resolutions. Because UV light cannot uniformly pass through the thick photoresist, thus the intensity of light in the bottom of the photoresist film decreases. It often results in a peel-off issue of the submicron structure with patterns because crosslinking densities of active materials at the bottom of films is low. Hayek et al suggested a greatly transparent epoxy-based photoresist, poly (glycidyl methacrylate) (PGMA), with highly decreased absorbance. As an alternative to SU-8, it is used to fabricate the 3D-photonic crystal structure through interference lithography using multi-beam.[10]

Polyhedral oligomeric silsesquioxane (POSS) is one of the interesting materials with an ultrahigh transparency, excellent mechanical properties, and good thermal stability due to the existence of cube-octameric framework consisting of RSiO1.5 functional groups.[11] It is expected that POSS-based polymer capable of photo-patterning functionalized with an acrylate or epoxy ring has improved transmittance. Also, they can be easily eliminated by heat treatments. Xu et al. introduced that silica template converted from POSS-based submicron structure can be easily eliminated by calcinations or O2 plasma etching.[12] Commercially available POSS-based photoresist has been widely utilized in previous studies. However, their glass transition temperature (Tg) are lower than room temperature. There is serious limitation on registration in the lithography because the polymer is in a liquid state at ambient conditions. Here, I introduce solid-type POSS-based photoresist with a high transparency that enables a fabrication of robust ultrathick submicron structures. To solve the main disadvantage of conventional photoresists, poly (glycidyl methacrylate-co-acryloisobutyl POSS) (PGP) is synthesized by polymerization of an acrylate monomer containing epoxy ring and transparent acrylate POSS containing silica compound. PGP displays an ultrahigh transmittance of light in UV-vis range (96.6 % at 355 nm of film with the thickness of 100 μm), a high Tg (~72.2 ℃), improved mechanical properties, low volume shrinkage, and easy elimination. Because of these properties of PGP, the proposed photoresists surpass the conventional photoresist such as SU-8, PGMA, commercially available POSS for the ultrathick patterned structure fabrication. This is the report to fabricate submicron patterns over 100 μm thickness by interference lithography. An ultrathick, large area, uniform PGP submicron structure has an improved mechanical property, resulting in providing outstanding potential in various applications.
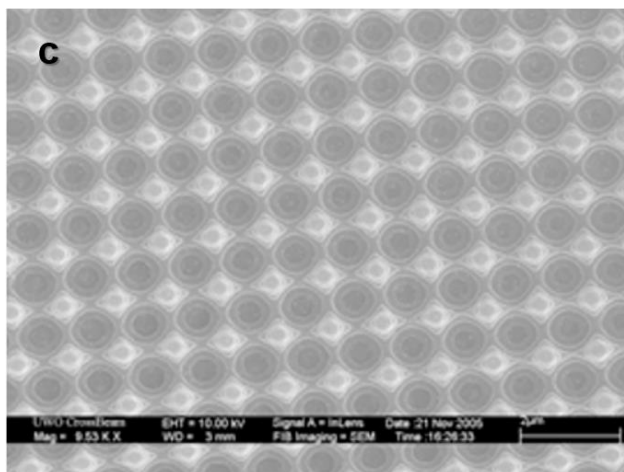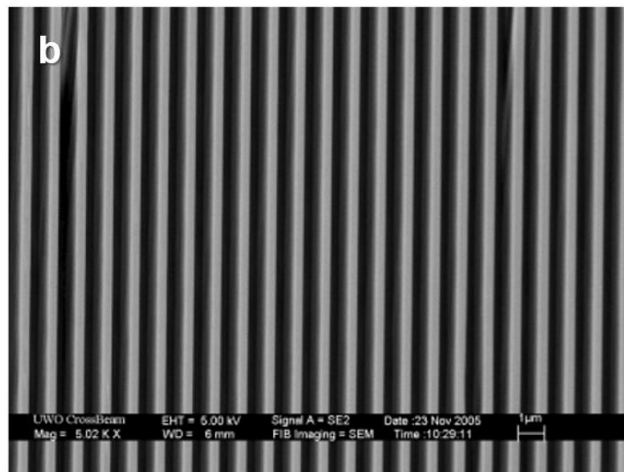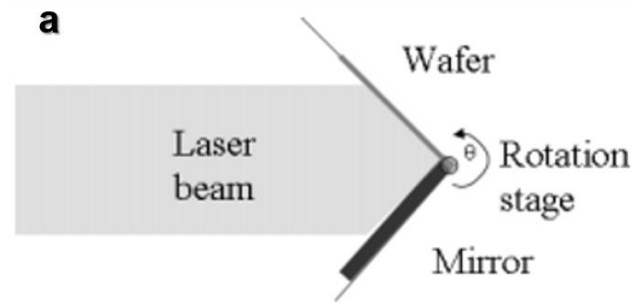
Fig. 1 a) Lloyd's mirror configuration of two-beam interference lithography. A SEM image of b) 1D interference pattern, c) pattern formed by double exposure.

13

1.2 Solar desalination

The earth is facing serious problems of water and fuel shortage. This problem is inevitable in the future due to population growth, development of modern industry and environmental pollution issue. Solar energy is free, pure, inexhaustible energy source and available in all regions including developing countries and remote zones without basic infrastructures. The three-quarters of the earth's surface is seawater, thus water is one of the most plentiful resources. Seawater desalinations that use the only solar energy without additional energy is promising in the future as a technique for freshwater supply.[13,15] Solar desalination occurs naturally as seawater heats up and has a minimal impact on the environment. This enables unlimited energy supply. However, this has the problem as a substitute technique to getting fresh water due to low light-to-heat conversion efficiency. Recently, researches have proceeded to efficiently desalinate under 1 sun solar irradiation.[16,17] Effective desalination technique has the following characteristics : hydrophilic surface, high absorption of photo-absorber in the solar spectrum range (from 300 to 2500 nm), low thermal conductivity for minimal heat losses, and an effective escape progress of created vapor bubbles.[18-20] Carbon nanotube (CNT) can maximize the light absorption in the full solar spectrum range, resulting in light-heat conversion efficiency is enhanced. The patterned structures could help trap the light by increasing the light increasing the light traveling through photo-absorber materials, resulting in increased light absorption. About 94 % solar-to-vapor conversion efficiency with a 1.78 kg/m^2 · h of evaporation rate is achieved under 1 sun illumination condition due to the synergistic effect of high absorption over the broadband sunlight wavelength and the large surface area of the PGP patterned structures.

II. Experimental methods

2.1 Fabrication of patterned structure

2.1.1 Materials

GMA was obtained from Alfa Aesar and used without further purification. Acryloisobutyl-POSS (A1-POSS) was purchased from Hybrid Plastics. AIBN was obtained from Samchun and purified by recrystallization from methanol. Distilled THF was used as a solvent for the synthesis reaction.

2.1.2 Polymerization

PGMA, PGP, and poly(acryloisobutyl POSS) (PAP) were synthesized by free radical polymerization utilizing an azobisisobutyronitrile (AIBN) as initiator. Monomers and initiator were dissolved in distilled THF. The solutions in which 20 wt% of the GMA and A1-POSS with 1 mM AIBN were dissolved in THF were heated to 65 $^{\circ}$C in a sealed ampoule under vacuum atmosphere. After 6 h., synthesized polymers were precipitated in isopropyl alcohol (IPA). Precipitation was repeated several times to completely remove the unreacted initiators and monomers. The precipitated polymers were gathered by filtration, washed several times with IPA, and then dried in the vacuum overnight. Finally, white powders were obtained.

2.1.3 Patterning with photoresist

Samples for the patterning of PGMAs and PGPs were prepared by the following procedure. 15 x 15 mm size of SiO_2/Si wafer was used as a substrate after washing step by step in acetone, IPA, D.I. water, and ethanol followed by N_2 blowing. A 30 wt% solution of the PGPs in cyclopentanone was spin-coated at a speed of 750 rpm for 1 min. The samples were prebaked at 75 $^{\circ}$C for 5 min. and then subsequently subjected to exposure of a Nd:YVO$_4$ laser in a Q-switched mode. A 44 mJ/cm^2 of the dose was exposed onto the sample (45 sec. of exposure time per single exposure) before post exposure bake (PEB) was applied at 75 $^{\circ}$C for 4 min.

2.1.4 Characterizations

Synthesized polymers were characterized by scanning electron microscopy (FEI Nano 230 and Hitachi High-Technologies S-4800), Fourier-transform infrared spectroscopy (FT-IR, Varian 670/620), nuclear magnetic resonance spectroscopy (NMR, Agilent 400-MR DD2), gel permeation chromatography (GPC, Wyatt miniDAWN TREOS), and UV-Vis spectroscopy (Agilent Cary 5000). Mechanical properties of submicron structures were investigated via nanoindentation (Hysitron Ti-750) using a Berkovich tip and the Oliver–Pharr method[1] to analyze the data to determine the respective Young's modulus and hardness values.

.

2.2 Solar desalination

2.2.1 Materials

Single wall carbon nanotube (SWCNT) dispersion solutions and nitric acid were purchased from KH chemicals and PFP, respectively. Sodium chloride for simulated seawater was purchased from Samchun chemical. All chemicals were utilized without any further purification.

2.2.2 Preparation of the photo-absorber materials

PGP and p-PGP film were prepared by the previous lithography process. SWCNT dispersion solutions were drop-coated on films and then dried. These were immersed in nitric acid for 12 hours. After acid treatment, these were washed several times with D.I water and then dried.

2.2.3 Characterization

The characterization was explored by scanning electron microscopy (Hitach High-Technologies S-4800), UV-Vis spectroscopy (Agilent Cary 5000). Hydrophilicity of photo-absorber was measured by contact angle measurement (Phoenix 300).

2.2.4 Steam Generation Measurements

The temperature and mass change by the evaporation of water for CNT, CNT/p-PGP on the bare wood and water only were investigated under the irradiation of simulated solar illumination (Sol2A class ABA 94062A, 1000W Xenon lamp, Newport) at a power density of 1 kW/m^2. The temperature was investigated using a thermographic camera and the mass change from evaporation was measured with an outer thermal insulation layer (about 1 cm-thick styrofoam) using an electronic microbalance with an accuracy of 0.1 mg every 1 minute. A square pillar shape wood piece with 1.5 cm thickness was floated on the surface of water in 5 ml cuvette with 1 cm diameter and 4 cm height

III. Results and Discussion

3.1 Patterned structure

Fig. 2 is a scheme of free radical polymerization with AIBN as an initiator for the synthesis of PGP. Glycidyl methacrylate (GMA) with the epoxy group and Acryloisobutyl POSS-functionalized acrylate group are polymerized at various feed-ratio in weight. **Table 1** shows the results of polymerization for PGP synthesis according to variation of amounts of POSS. GMA was used as a negative-type photoresist due epoxy groups is crosslinkable upon exposure. The transparency, and mechanical stability of the synthesized polymer were enhanced due to the introduction of the acryloisobutyl POSS with $-Si-O_{1.5}-$ cube-octameric frameworks. PGMA resin has good chemical resistance and high mechanical properties so it has been extensively utilized as photoresists, printing inks, printing plate and coatings. Because PGMA exhibits low volume shrinkage and relatively high transparency, we used it as a backbone photoresist polymer. The inorganic cage segment of POSS improves the transparency and mechanical stability of prepared photoresist polymer.[21] This photoresist could be utilized to fabricate robust and thick submicron structures. On the other hand, the functional group of POSS dilutes the dipole-dipole interactions of GMA monomers, so the glass transition temperature (T_g) of synthesized PGP was decreased as the amount of POSS increases as shown in **Fig. 3a**.[22] T_g value is one of the important properties for photoresist because photoresist remains in a solid phase and it is applicable to a variety of lithography method. Because a liquid-type photoresist produces adverse effects such as unstable contact between the resist and the mask and distortion of the incident light in the flux materials. Besides, the low T_g value of the photoresist causes problems including pattern distortion, diffusion acid during the process at the high temperature (e.g. PEB). A solid-type photoresist having high T_g was obtained by controlling the POSS content. Differential scanning calorimetry (DSC) data in **Fig. 3b** shows the thermal properties of PGPs with the various amount of POSS. The T_g values of PGMA and PGP-2 (~76.2 °C and ~72.2 °C, respectively) were much greater than room temperature, compared to the low T_g value (~2 °C) of the epoxy-functionalized POSS photoresist. Synthesized photoresist is a solid phase status at room temperature, resulting in it is durable under high temperature process conditions. The thermal stability of PGP was explored by TGA data, as shown in **Fig. 3c**. This indicated that PGP is thermally stable even at 250 °C, which is above the process temperature.
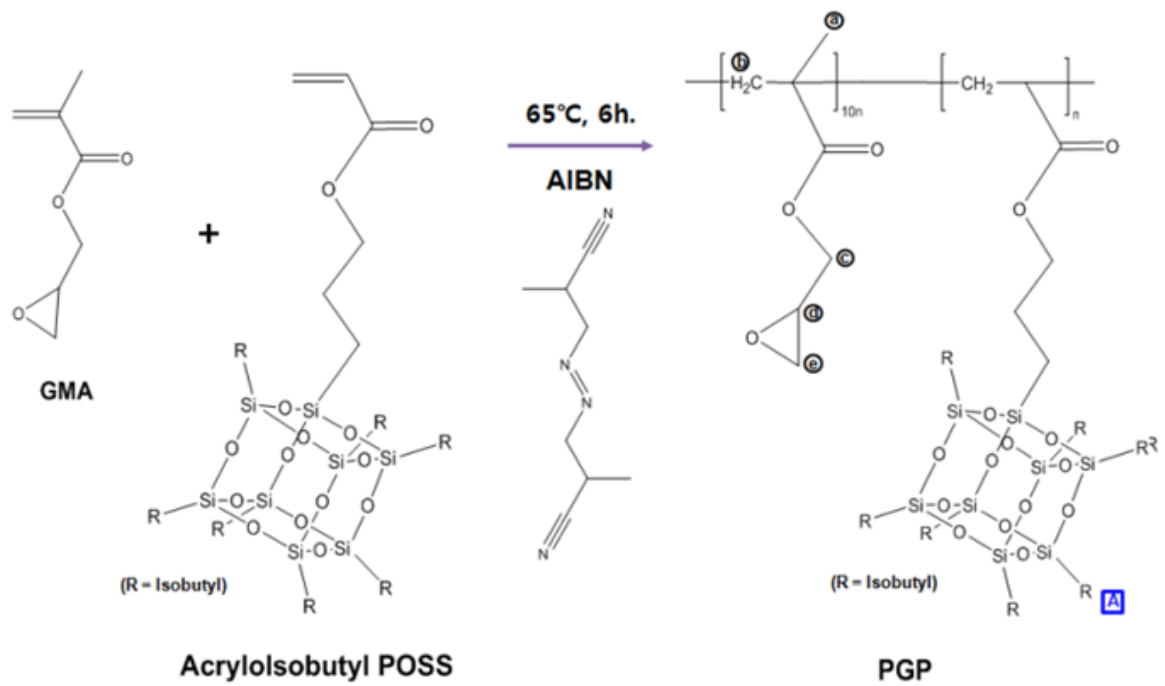
Fig. 2 Scheme of the synthesis via the polymerization reaction of PGP-2 (R= isobutyl group).

	Feed ratio (POSS mol%)	Product ratio (POSS mol%)	Initiator (mol%)	M_w	DP
PGMA -1	0	0	0.05	143k	1006
PGMA -2	0	0	0.1	101k	710
PGP-1	4.76	1.56	0.1	110k	712
PGP-2	9.09	3.03	0.1	157k	950
PGP-3	16.67	5.56	0.1	136k	732
PAP	100	100	0.1	4,791	5

Table 1. The analysis of polymerization results for synthesized polymers via GPC and H-NMR data.
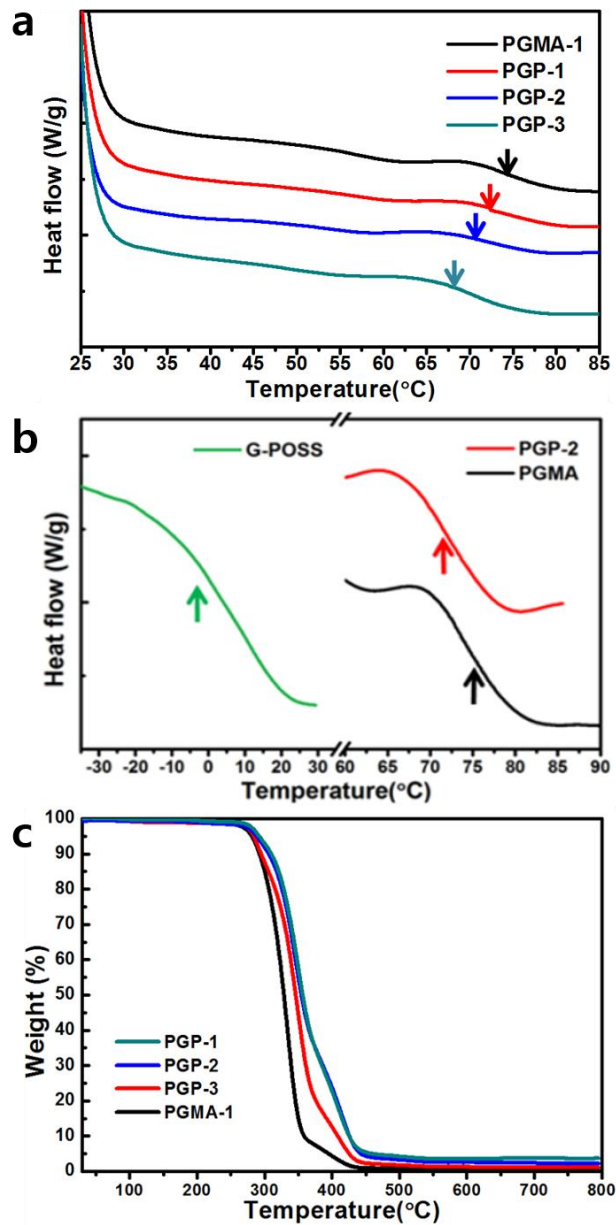
Fig. 3 a) T_g values of PGMA and synthesized PGPs via Differential scanning calorimetry (DSC), b) DSC data of G-POSS, PGP-2, PGMA, c) Thermogravimetric analysis (TGA) data of synthesized PGPs.

20

As shown in **Fig. 4a**, the transmittance of the PGP-2 film with the thickness of 100 μm is about 96.6 % at 355 nm, which is the wavelength of the irradiated laser. Moreover, the transmittance spectra of the various thickness films were shown in **Fig. 4b**. The transmittance of 127 μm-ultrarhick PGP-2 film was higher than that of PGMA with the thickness of 83μm and SU8 with the thickness of 50 μm at 355 nm. **Fig. 5a and b** show the spectra of Proton nuclear magnetic resonance (1H-NMR) and Fourier transform infrared (FT-IR) of synthesized polymers**.** Each proton marked in a chemical structure shown in **Fig. 2** corresponds to the 1H peaks of PGP-2 shown in **Fig. 5a**. As shown in **Fig. 5b**, the C–H vibration from a back bone of polymers and the C=O stretching of the ester carbonyl groups corresponds to the peaks at 2900 cm^{-1} and a strong vibrational band at 1728 cm^{-1} in FT-IR spectra. The epoxy ring of GMA and the Si-O-Si linkage, which is illustrated by the blue square in **Fig. 2** are assigned to usual absorption bands at 910 cm^{-1} and at 1128 cm^{-1}. These peaks confirm that POSS incorporated in PGP synthesis. To obtain both high transparency and T_g, the content of POSS to GMA was optimized approximately 3.03 % of the molar ratio (PGP-2, **Table 1**). The product mole ratios of the GMA monomer were calculated from the intensities of the peak at 3.2 ppm and 0.6 ppm for GMA and A1-POSS, respectively in **Fig. 5a**. All product mole ratios are approximately one-third of the feed ratios due to the reduction of free radical copolymerization reactivity. This is because of steric hindrance caused by the bulky and rigid part of A1-POSS macromonomers.[23] Overall, we discovered that POSS has a substantial impact on significant properties of PGP as a photoresist, including T_g, transparency and the molecular weight. The introduction of POSS into the PGP polymer cause in a decrease in T_g but an increase in weight average molecular weight and transmittance.
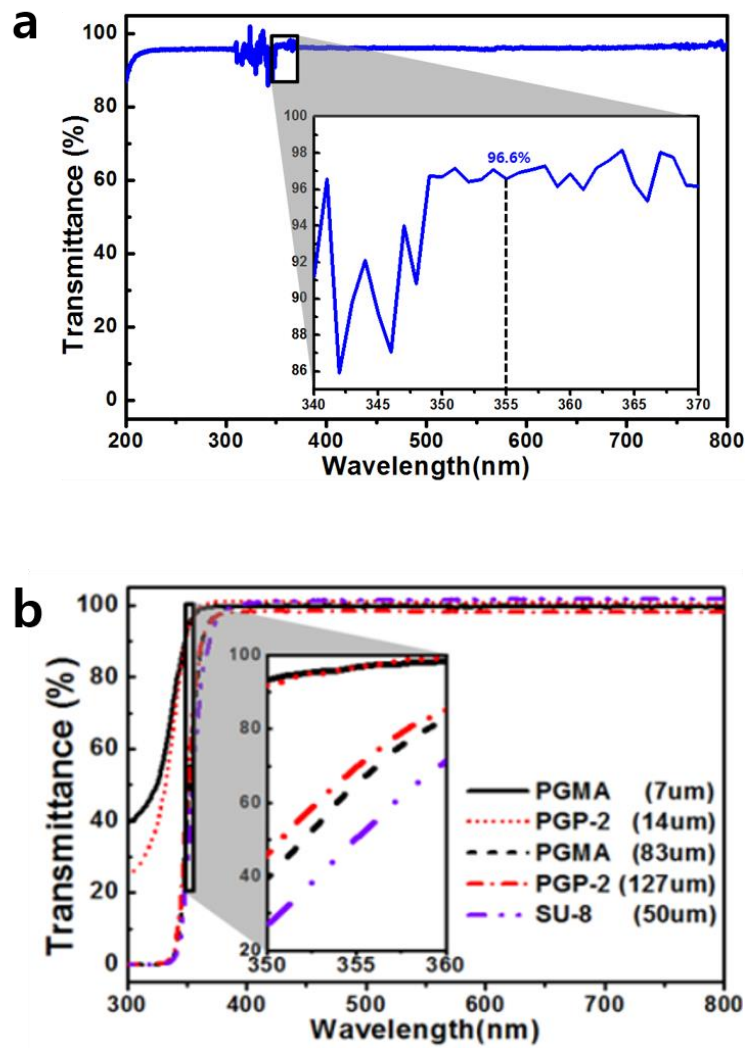
Fig. 4 a) The transmittance spectra of the PGP film with the thickness of 100 μm confirmed via UV-Vis spectrophotometer, b) UV-Vis spectrometry of films synthesized PGPs and SU-8.
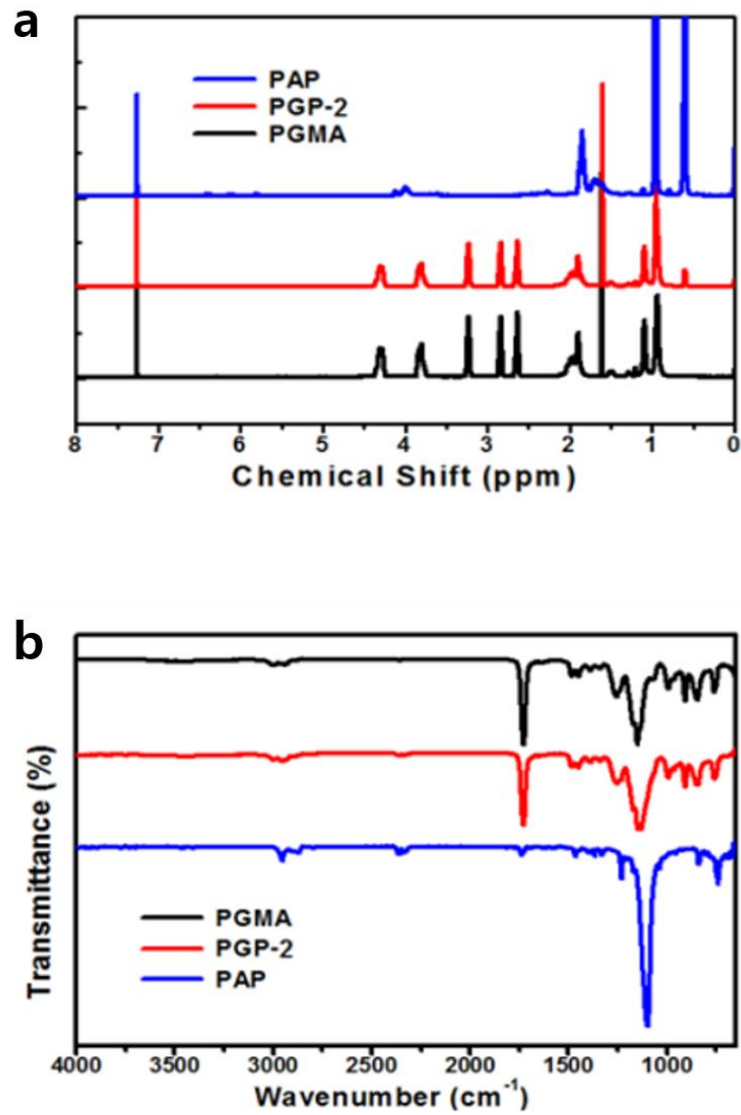
Fig. 5 Characterization of PGMA, PGP-2, PAP by a) proton NMR, b) Fourier-transform infrared spectroscopy (FT-IR).

23

Fig. 6 shows the result of measuring the mechanical strength of PGMA and PGP-2 film with squared patterns using nanoindentation. Using a Bekovich tip, the PGMA and PGP-2 films with squared patterns was indented up to a maximum load of 500 mN at the constant $\dot{P}/P$ (the nominal strain rate of 0.05 s^{-1}). An Oliver and Pharr method was used to analyze a load-displacement curves of PGMA and PGP-2 film with square patterns shown in **Fig. 6a**. **Fig. 6b-c** show the result of Young's modulus (E) and the hardness (H) that were taken at 15 % of the film thickness or 1.5 μm of indentation displacement, to avoid substrate effects.[24] The results of PGP-2 were H = 0.16 GPa and E = 6.09 GPa, respectively, which are 10 % and 17 % higher than those of the patterned PGMA, respectively. I assume that Young's modulus and hardness have increased because it contains more rigid POSS molecules than the PGMA. Thus, it is possible to improve Young's modulus and mechanical strength and also ensure the transmittance required as a photoresist by including POSS molecules. H = 0.16 GPa and E = 6.09 GPa of the PGP-2 submicron patterned structure are 8 and 4.2 times higher than SU8 nanopatterns, respectively. A uniform distribution of POSS molecules in PGP polymers enhances Hardness and Young's modulus by providing uniform delocalization of a load.[25] In comparison with PGMA, PGP has the improved transmittance, mechanical properties as a photoresist due to inclusion of inorganic POSS. The introduction of POSS in the PGP is expected to enhance the Hardness and young's modulus of PGP in compliance with its volume fraction, where $E = xA + (1 − x)B, H = xA + (1 − x)B$. 'x' is a volume fraction of POSS in the prepared PGP, and 'A' and 'B' are the mechanical strengths of POSS and PGMA, respectively.
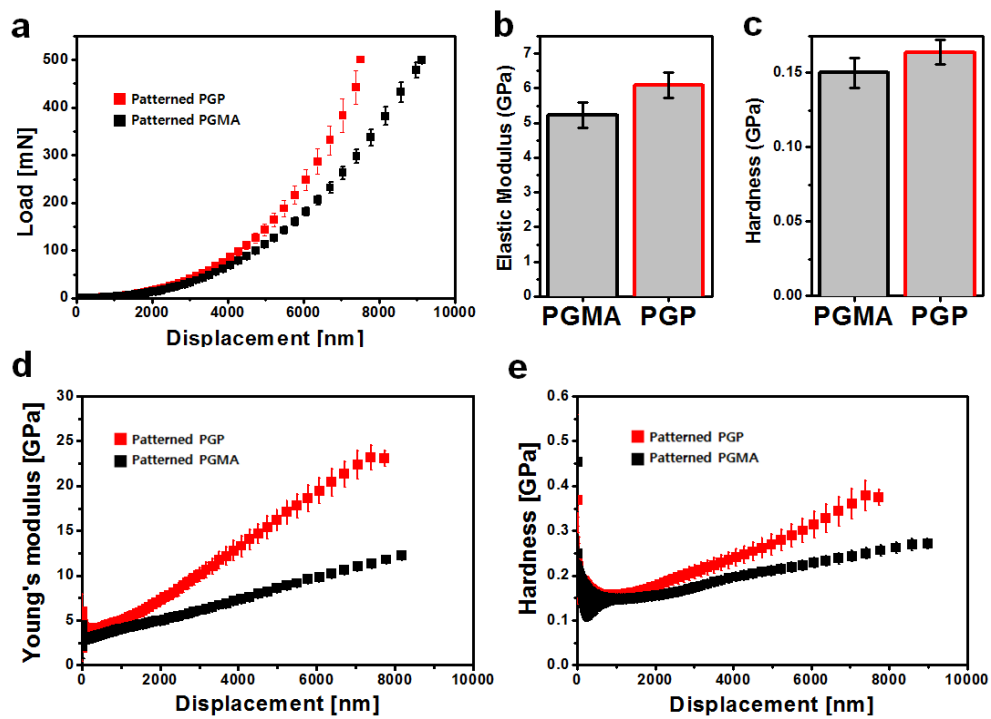
Fig. 6 Mechanical strengths of PGMA and PGP-2 film with the square pattern. a) Load-displacement curves of PGMA and PGP-2 film with patterned structures of maximum load of 500 mN. b) Young's modulus and c) Hardness that are explored by Oliver-Pharr nonlinear curves fit method. d) Young's modulus-displacement curves and e) Hardness-displacement curves that were taken at 15 % of the film thickness or indentation displacement of 1.5 μm.

We assumed that the submicron structure with an extremely high-aspect ratio in the large area could be fabricated because of the excellent mechanical properties and high transmittance of optimized PGP. Using prepared PGP as a photoresist, we were able to successfully fabricate the ultrathick submicron structures with the thickness of 105 μm and an aspect ratio of 131 via interference lithography. (The patterned structures at 150 μm-height shows slightly twisted and collapsed morphology in **Fig. 7c and d**.) Multi-beam interference lithography is an easy technique to fabricate structures that have a periodic pattern, defect-free in relatively large areas. Here, two-beam interference lithography was utilized to fabricate uniform ultrathick submicron structures over the large area. The fabrication includes irradiating a laser beam of the same intensity twice in succession while rotating the sample 90 degrees. The irradiated light leads to pattern formation through cationic polymerization of the epoxy group in photoresist polymer. **Fig. 7a** displays the top surface image of the submicron structure with a periodic pattern of a hole diameter of ~800 nm square lattice with pitch of 1.8 μm. (A use of a negative-type photoresist and interference lithography determined the limitation of geometry of the square pattern. The inset shows a high magnification image of well-defined patterns.) The cross-sectional image in **Fig. 7b** indicate the ultrathick submicron structure formation. As shown in **Fig. 7b**, the reason for the formation of highly uniform and neatly hole with a cylindrical shape from top to bottom of the photoresist film with the thickness of 100 μm is the improved mechanical strength and transmittance of the synthesized PGP polymer. We applied PGP to another lithography technique to fabricate 3D-submicron structures. **Fig. 8** shows that 3D holographic submicron structure with the thickness of 83 μm was successfully fabricated via the proximity field nanopatterning (PnP) method. This result indicates that it is possible to fabricate ultrathick submicron structure via other lithography techniques by using PGP photoresist. A volume shrinkage of the photoresist was calculated by the following equation using the film thickness measured through cross section views of SEM images before and after patterning steps.

$$\text{Shrinkage} = \left(1 - \frac{\text{thickness of patterend film}}{\text{thickness of unpatterned film}} \right) \times 100 \ (\%)$$

Shrinkage occurs because an intermolecular distance between monomer units needed to keep thermodynamic equilibrium condition during a monomer/cross-linked polymer transformation is reduced. A substantial distortion in the final shape of structures, poor adhesion to the substrate and resolution reduction are problems caused by large volume shrinkage. The volume shrinkage of PGMA and SU-8 were 3.13 % and 40.8 %, respectively, while those of PGP-2 was 2.36 %. The reason for the low volume shrinkage of PGP is that the inorganic cage of POSS compound has a filler strengthening effect and an interpenetrating effect.
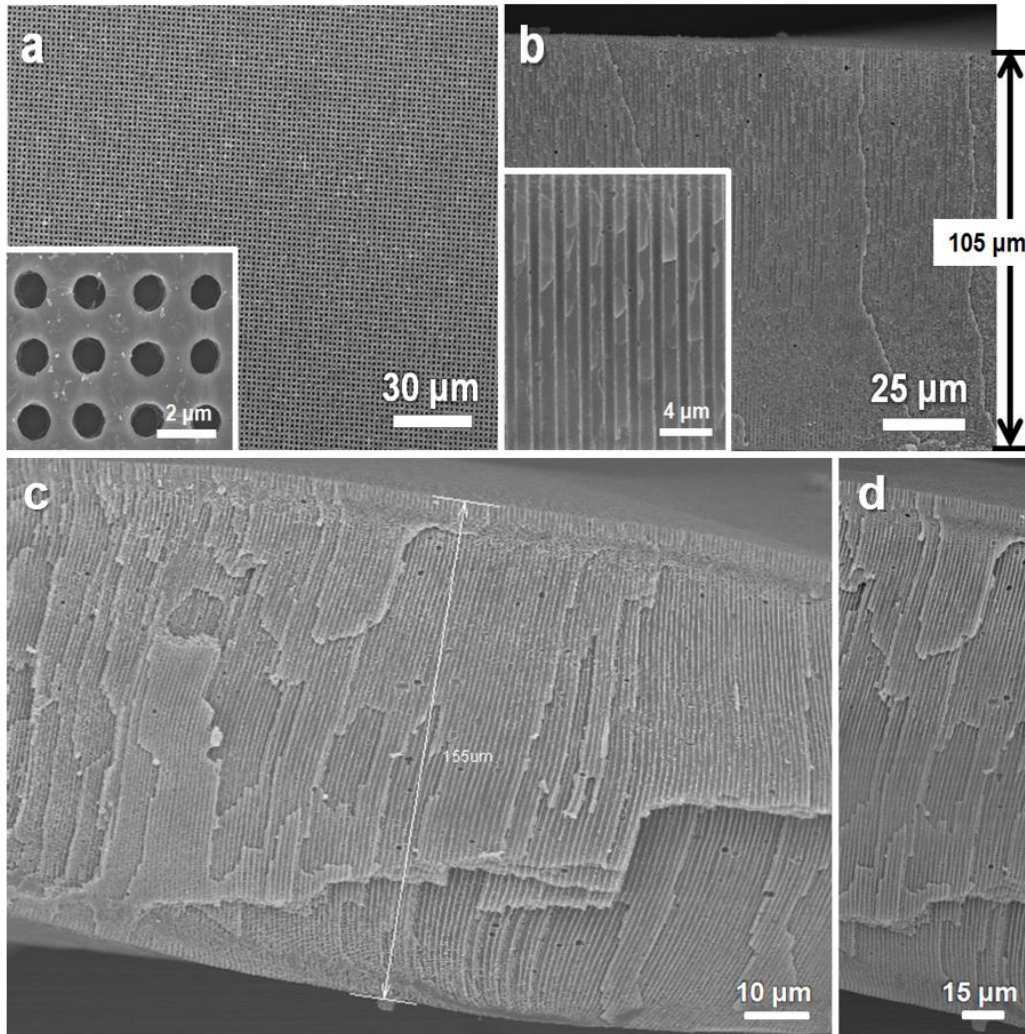
Fig. 7 Scanning electron microscopy (SEM) images of square patterned PGP structures with the thickness of 105 μm. a) Top view. b) Side view. (The insets are high magnification images.) c, d) a square patterned submicron structure over 150 μm.
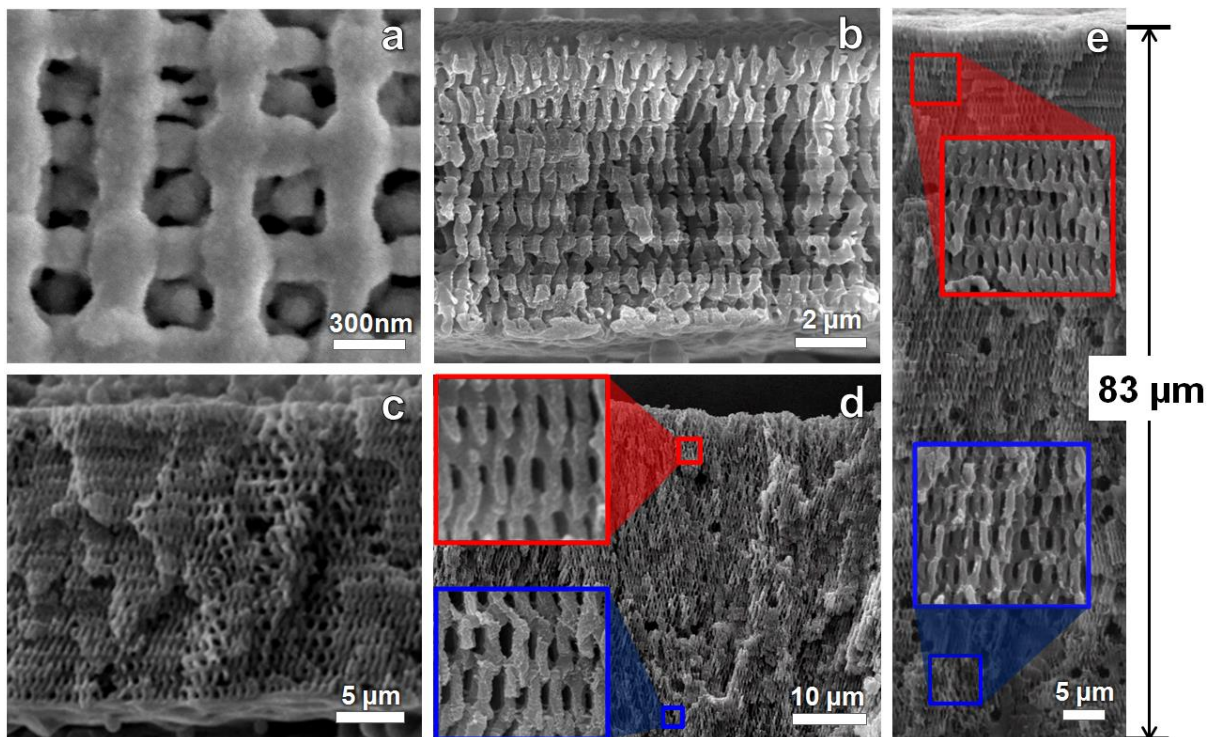
Fig. 8 SEM images of the holographic patterned submicron structures with various thicknesses. a) Top view and cross-section view of b) 8 μm, c) 20 μm, d) 50 μm and e) 83 μm. The inset is the high magnification image.

3.2. Solar desalination

Two dimensional periodic patterns provide water transport and generated vapor escape paths in the solar desalination process. Periodic patterns also help sunlight absorption of photo-absorber materials enhanced due to multiple scattering. To efficient steam generation via thermal evaporation, the solar desalination device should contain the active material that absorbs a lot of light and can effectively convert energy from sunlight to heat. However, **Fig 10a and b** show high transmittance and low absorption of PGPs ultrathick patterned film in the broadband solar spectrum range from 300 to 2500nm wavelength. In order to enhance absorption of sunlight, Carbon nanotube (CNT) having ultrahigh absorption was drop-coated on the patterned film, as shown **Fig 9a and b**. While the PGP film exhibited around 0% of absorption value, CNT/PGP film and CNT/p-PGP film exhibited high absorption exceeding 90% in the solar spectrum range **in Fig 10b.** Moreover, Absorption of CNT/p-PGP film was slightly higher than that of CNT/PGP film. This is because periodic patterns trap the light by increasing the light traveling via light scattering. This confirmed by diffuse reflectance spectra in **Fig 9d**. After coating the CNT, that material was acid treated by soaking in nitric acid solution. Hydrophilicities of CNT-PGP films before and after acid treatment were confirmed by a contact angle investigation as shown in **Fig 11**. Un-acid treated PGP film and CNT/PGP film has a high contact angle of 84 ° and 92 °, respectively, in **Fig 11a and b**. In the case of an acid treated CNT-PGT film in **Fig 11c**, as soon as the water drops, it spreads on the film. This means hydrophilicity is greatly enhanced by acid treatment, resulting in water transfer effectively generating.
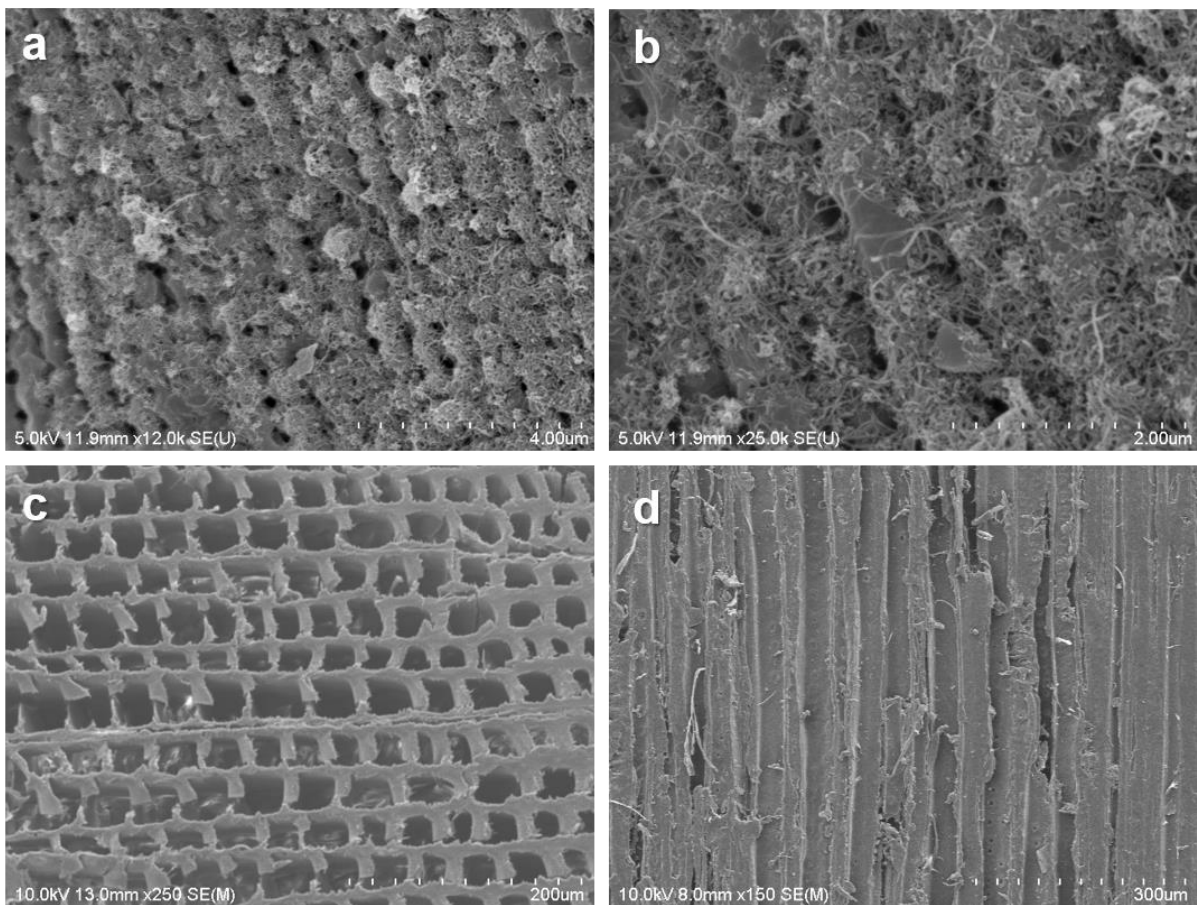
Fig. 9 SEM images of a) Carbon nanotube (CNT) coated on the patterns and b) magnification images. C) Top view and d) Side view of the wood piece.
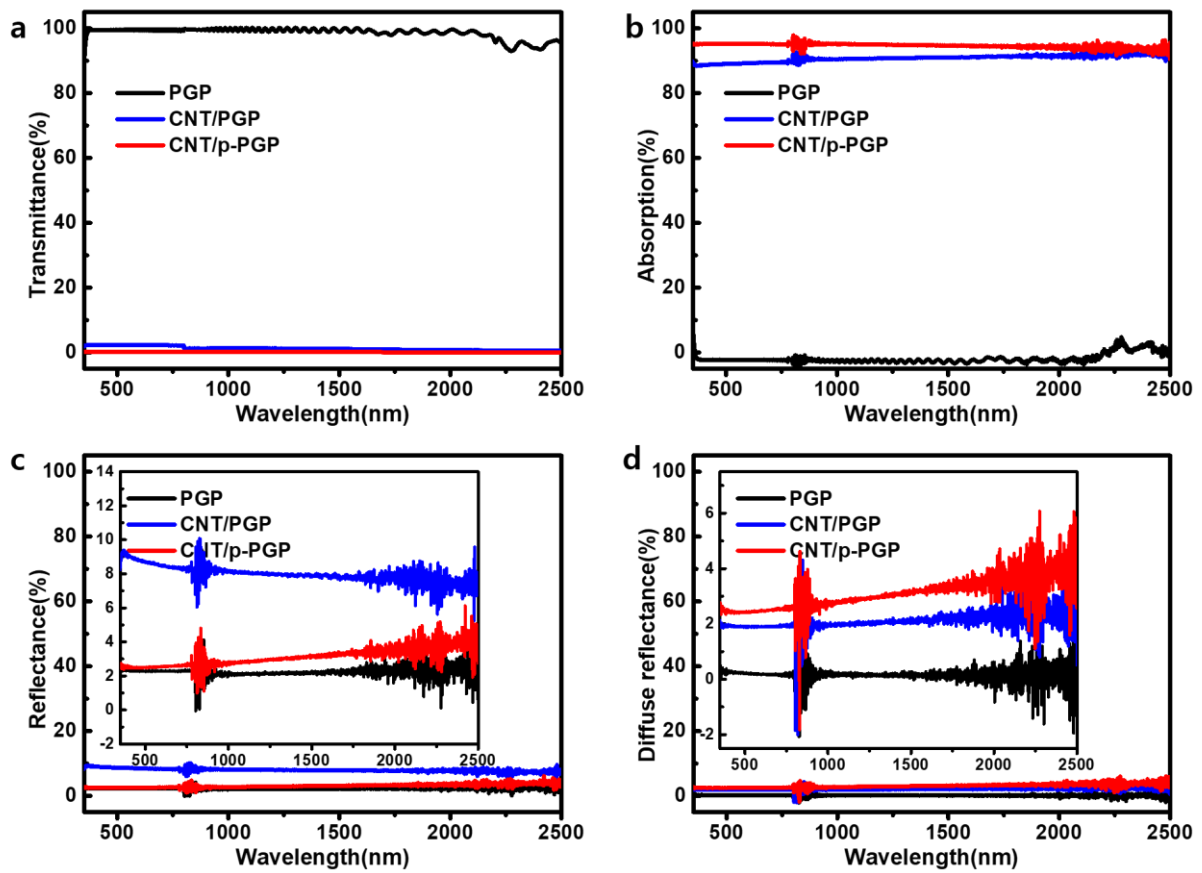
Fig. 10 UV-Vis spectroscopy of PGP film, CNT/PGP film and CNT/p-PGP film. A) Transmittance b) Absorption (Absorption (%) = 100 – Transmittance (%) – Reflectance (%)) c) Reflectance d) Diffuse reflectance.
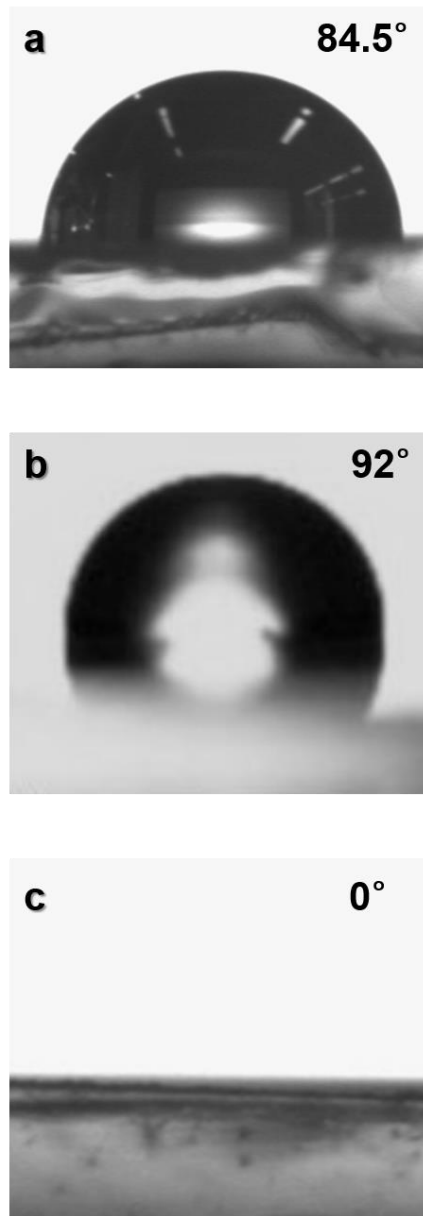
Fig. 11 Contact angle of a) PGP film, b) (un-acid treated) CNT/PGP film, c) (acid treated) CNT/PGP film.

The wood piece has a path to transport water using capillary force. As shown in **Fig 9c and d**, the wood has tubular structure aligned vertically with vessels of a few tens of micrometer. The wood piece also restrict heat transfer from the active material to bulk seawater. Because the thermal conductivity of wood is very low (~0.02 W/Mk).[27] Since bulk water does not need to be heat, the heat loss in bulk water decreases the solar-to-vapor efficiency. The steam is generated via thermal evaporation on the top of bulk water in which the active material is present.[28] As shown in the digital camera image in **Fig. 12 a**, CNT/p-PGP placed on the wood was floated on the saline water. We placed the prepared solar desalination devices under a solar simulator at about 20 % humidity and 20 °C. After illuminating at 1 sun for 1 hour, the temperature on the surface of the bare wood and CNT/p-PGP film increased to around 27 °C and 37 °C, respectively, as shown in **Fig 12 b, c and d**. The temperature on the bare wood is lower than that of CNT/p-PGP film since the photo-thermal conversion mechanism does not operate. CNT/p-PGP showed a large temperature increase due to effective photo-thermal conversion efficiency. As the wood piece not only transports water but also localizes the heat only on the wood, there is a difference in temperature between top of the wood and bottom of the devices. The temperature of the surface of photo-absorber is lower than that of the wood since the heat generated evaporates the water. By combining the high absorption of photo-absorber and heat localization of wood, the temperature of devices increases under 1 sun illumination caused the active evaporation of water, as shown in **Fig. 12 c and d**. As shown in **Fig 13**, the mass change of 3.5% saline water was measured to calculate the solar-to-vapor conversion efficiency of CNT/PGP, CNT/p-PGP under simulated solar illumination 1 Kw/m^2, All evaporation rates were calculated at steady state after simulated sunlight was illuminated for 1 hour. At a solar intensity of 1Kw/m^2, the mass change rate of CNT/p-PGP on the wood piece was as high as 1.78 kg/ · h, which is about 4 times greater than that of saline water only of 0.48 kg/ · h. The mass change rate of the bare wood was only 1.26 kg/ · h, indicating that the high sunlight absorption of photo-absorber materials plays an important role. The CNT/PGP on the wood presents mass change of 1.45 kg/ · h because lower sunlight absorption without light scattering effect of patterned structure (**Fig. 10 b and c**).

The solar-to-vapor conversion efficiency () was calculated by the followed equations:

$$\eta = \frac{Q_e}{AC_{opt}Q_s}, Q_e = m\lambda + mC \triangle T$$

Where Q_s denotes the intensity of normal direct solar irradiation (1 Kw/m^2), C_{opt} denotes the optical concentration, and A denotes the cross-sectional area of light illumination. Q_e is the power consumed for the steam generation, C denotes the specific heat capacity of water (4.2 J/g · K), and m denotes mass flux by the energy converted from solar to heat only without natural evaporation in a dark condition (no illumination). $\triangle T$ is the temperature increases of the water, and λ denotes the latent heat of the phase change from water to vapor. **Fig. 13b** shows efficiency of pure water was 15.7% under an illumination of 1 Kw/m^2. A large temperature difference by efficient thermal insulation effect, vapor escape channel is important to generate vapor molecule and to escape vapor molecule into the air. These properties affect effective solar-to-vapor conversion of photo-absorber, which directly related to evaporation rate. The evaporation rates tended to correspond with these properties of the photo-absorber materials (CNT/PGP, CNT/p-PGP), as already confirmed. CNT/PGP and CNT/p-PGP on the wood has an efficiency of 78.5 %, 94.1 %, respectively. The evaporation rate and solar-to-vapor conversion of CNT/p-PGP were much higher than those of CNT/PGP due to the increased light absorption and the vapor escape channel of patterned structures. Although the absorption of two photo-absorbers is similar in the absorption for the full sunlight spectrum range, the reason for the difference in the evaporation rate and effective solar-to-vapor conversion Although absorption of the two photo-absorbers was similar in the full sunlight spectrum range, CNT/p-PGP on the wood piece appears greater evaporation rate and effective solar-to-vapor conversion due to the vapor escape channel of CNT/p-PGP.

b	Before sunlight illumination	After sunlight illumination for 1 hour
Bare wood	20 ℃	27 ℃
CNT/p-PGP on the wood	20 ℃	37 ℃
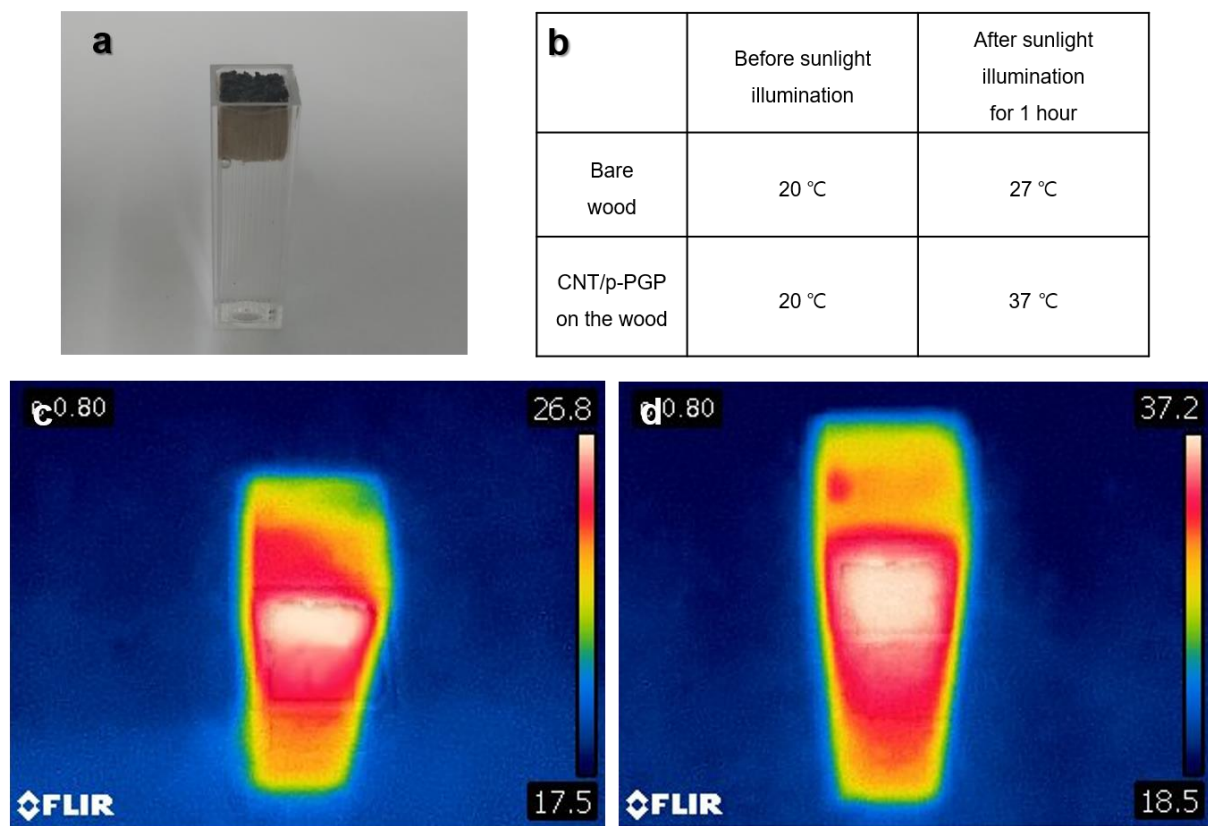
Fig. 12 a) DC image of CNT/p-PGP film on the wood piece, b) temperature changes at the wood piece of bare wood and CNT/p-PGP film on the wood piece, thermographic images of c) bare wood and d) CNT/p-PGP film on the wood piece.

Fig. 13 a) Mass changes of water in solar desalination devices containing CNT/PGP, CNT/p-PGP on the woods as a function of time under solar illumination of $1\ \mathrm{Kw}/m^2$. b) Solar-to-vapor conversion efficiency calculated by the mass change rate after illuminating sunlight for 1 hour.

IV. Conclusions

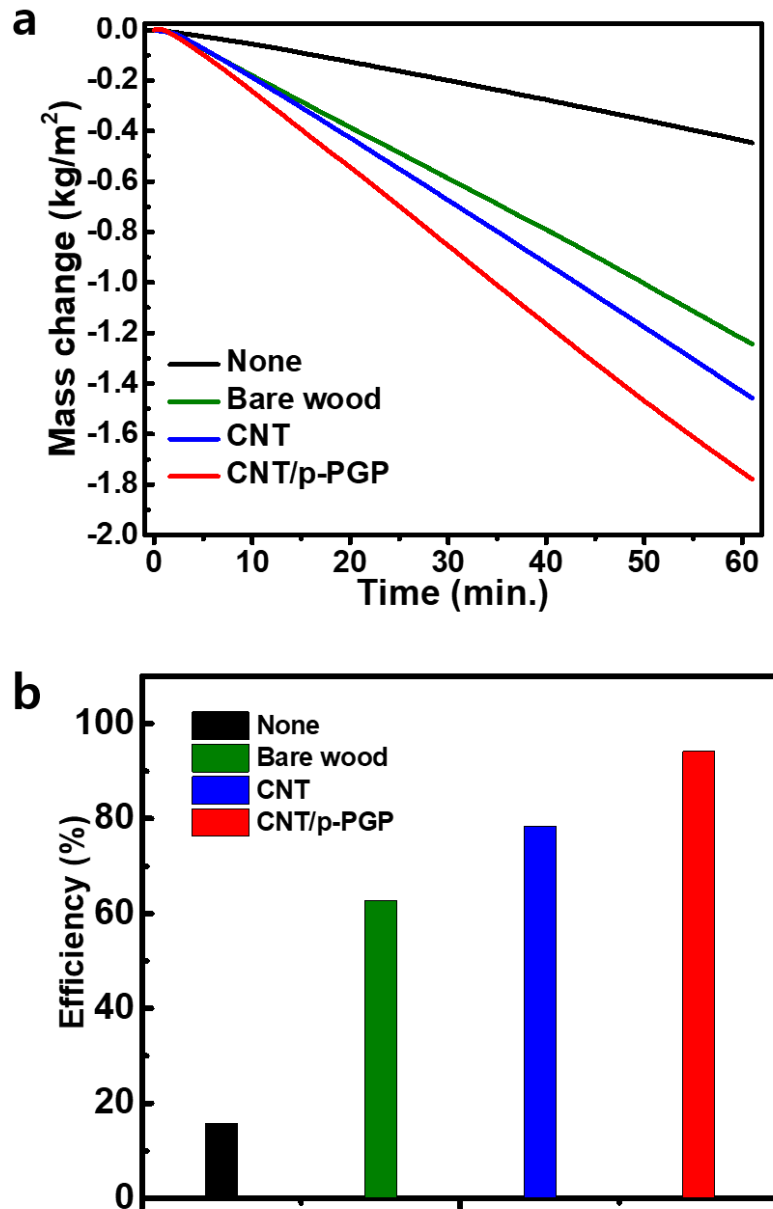PGP is a new solid-state POSS based photoresist with photo-active, mechanically robust, and highly transparent. It was synthesized by free radical polymerization and enables the fabrication of patterned structure with thickness higher than 100 μm and the aspect ratio of over 100. As a photoresist for the ultrathick submicron structure, the amount of POSS in the PGP polymer was optimized by considering transmittance and the T_g value. The mechanical strength of the PGP film with submicron patterns showed the hardness of 0.16 GPa and Young's modulus of 6.09 GPa, which were 8 and 4.2 times, respectively, higher than those of SU8 film with nanopattern. PGP can be a great substitute for the widely utilized SU8. These 3D-ultrathick submicron structures having improved mechanical strength can serve as a robust material platforms for microfluidics, MEMS, and other applications. Solar desalination, one of the applications, is a technique to desalinate water using solar energy. CNT/p-PGP exhibits excellent photo-absorption of over 90 % at the broadband wavelength of sunlight and has a patterned structure which helps vapors to easily nucleate and escape into the air. Therefore, It has optimum properties as photo-absorber in desalination device. CNT/p-PGP on a wood can serve as an efficient solar desalination device with high solar-to-vapor conversion efficiency of over 94% under the 1 sunlight illumination condition (1 kW/m^2). It can be an uncomplicated solution for the serious global water shortage issue.

Reference

1. Y. Xu, X. Zhu and S. Yang, *ACS Nano*, 2009, **3**, 3251-3259.

2. J. Li, G. Liang, X. Zhu and S. Yang, *Adv. Funct. Mater.*, 2012, **22**, 2980-2986.

3. K. Kim, M.-J. Kim, S.-I. Kim and J.-H. Jang, *Sci. Rep.*, 2013, **3**, 3330.

4. S. Hyun, O. Kwon, B.-y. Lee, D. Seol, B. Park, J. Y. Lee, J. H. Lee, Y. Kim and J. K. Kim, *Nanoscale*, 2016, **8**, 1691-1697.

5. K. Kim, J. Lee, G. Jo, S. Shin, J.-B. Kim and J.-H. Jang, *ACS Appl. Mater. Interfaces*, 2016, **8**, 20379-20384.

6. K. Kim, P. Thiyagarajan, H.-J. Ahn, S.-I. Kim and J.-H. Jang, *Nanoscale*, 2013, **5**, 6254-6260.

7. J. H. Jang, C. K. Ullal, M. Maldovan, T. Gorishnyy, S. Kooi, C. Koh and E. L. Thomas, *Adv. Funct. Mater.*, 2007, **17**, 3027-3041.

8. C. Lu and R. H. Lipson, *Laser photonics Rev.*, 2010, **4**, 568-580.

9. S. Ghosh and G. Ananthasuresh, *Sci. Rep.*, 2016, **6**, 18428.

10. A. Hayek, Y. Xu, T. Okada, S. Barlow, X. Zhu, J. H. Moon, S. R. Marder and S. Yang, *J. Mater. Chem.*, 2008, **18**, 3316-3318.

11. H. Zhou, Q. Ye and J. Xu, *Mater. Chem. Front.*, 2017, **1**, 212-230.

12. Y. Xu, M, Guron, X. Zhu, L. G. Sneddon and S. Yang, *Chem. Mater.*, 2010, **22**, 5957-5963.

13. M. Fujiwara and T. Imura, *ACS Nano*, 2015, **9**, 5705-5712.

14. M. Gao, P. K. N. Connor and G. W. Ho, *Energ Environ. Sci.*, 2016, **9**, 3151-3160.

15. H. Ren, M. Tang, B. Guan, K. Wang, J. Yang, F. Wang, M. Wang, J. Shan, Z. Chen, D. Wei, H. Peng and Z. Liu, *Adv. Mater.*, 2017, **29**, 1702590.

16. M. Fujiwara and T. Imura, *ACS Nano*, 2015, **9**, 5705-5712.

17. M. Gao, P. K. N. Connor and G. W. Ho, *Energy Environ. Sci.*, 2016, **9**, 3151-3160
.

18. H. Ren, M. Tang, B. Guan, K. Wang, J. Yang, F. Wang, M. Wang, J. Shan, Z. Chen, D. Wei, H. Peng and Z. Liu, *Adv. Mater.*, 2017, **29**, 1702590.

19. S. Yu, Y. Zhang, H. Duan, Y. Liu, X. Quan, P. Tao, W. Shang, J. Wu, C. Song and T. Deng, *Sci. Rep.*, 2015, **5**, 13600.

20. Y. Li, T. Gao, Z. Yang, C. Chen, W. Luo, J. Song, E. Hitz, C. Jia, Y. Zhou, B. Liu, B. Yang and L. Hu, *Adv. Mater.*, 2017, **29**, 1700981.

21. N. Xu, X. Hu, W. Xu, X. Li, L. Zhou, S. Zhu and J. Zhu, *Adv. Mater.*, 2017, **29**, 1606762.

22. D.-Y. Kang, S. Lee and J. H. Moon, *RSC Adv.*, 2014, **4**, 32348-32352.

23. E. Ayandele, B. Sarkar and P. Alexandridis, *Nanomaterials*, 2012, **2**, 445.

24. L. Hong, Z. Zhang, Y. Zhang and W. Zhang, *J. Polym. Sci., Part A: Polym. Chem.*, 2014, **52**, 2669-2683.

25. S. M. Han, R. Saha and W. D. Nix, *Acta Mater.,* 2006, **54**, 1571-1581.

26. M. M. Demir, B. Altın and S. Özçelik, *Compos. Interfaces*, 2010, **17**, 831-844.

27. S. Lee, Y.-C. Jeong, J. Lee and J.-K. Park, *Opt. Lett.*, 2009, **34**, 3095-3097.

28. G. Xue, K. Liu, Q. Chen, P. Yang, J. Li, T. Ding, J. Duan, B. Qi and J. Zhou, *ACS Appl. Mater. Interfaces*, 2017, **9**, 15052-15057.

29. Y. Liu, S. Yu, R. Feng, A. Bernard, Y. Liu, Y. Zhang, H. Duan, W. Shang, P. Tao, C. Song and T. Deng, *Adv. Mater.*, 2015, **27**, 2768-2774.

Acknowledgements

저의 석사 생활을 끝마치면서 감사의 인사를 드려야 할 분들이 많은 것 같습니다. 저의 지도 교수님이신 장지현 교수님께 제일 먼저 감사하다고 전해드리고 싶습니다. 대학원에 막 입학했을 때에는 부족한 것이 많았지만 석사 생활 동안 교수님의 지도를 받으면서 많은 것을 배울 수 있었습니다. 대학원을 졸업하고 나서도 교수님의 지도를 잊지 않고 있겠습니다. 더불어 저의 석사 학위 졸업 논문을 심사해주신 박성훈 교수님, 장지욱 교수님께도 감사하다고 전하겠습니다. 교수님들께서 해주신 조언, 충고들이 저에게 많은 도움이 되었습니다. 마지막으로, 저의 석사 생활 동안 힘이 되어준 우리 실험실 친구, 언니, 오빠들 고맙습니다. 아무것도 모르던 저에게 많은 것을 알려주느라 고생한 저의 사수 광현 오빠, 타지 생활이 처음인 저에게 많은 힘이 되어준 제 룸메이트 성지 언니, 대학원에 막 진학했을 때부터 학부 후배인 저를 많이 신경 써준 종하 오빠, 더불어 긴 말을 적지 못했지만 종철 오빠, 성욱 오빠, 기용 오빠, 진욱 오빠, 지훈 오빠, 경남 오빠, 주형이, 세영이, 철원 오빠, 재은 언니, 수희까지 모두들 감사했습니다. 여러분 덕분에 실험실 생활 동안 잘 지낼 수 있었고 무사히 끝마칠 수 있었습니다. 감사의 인사 전해드린 모든 분들 항상 건강하시고 하시는 일들이 모두 잘 되었으면 좋겠습니다.